

# Gapped broken symmetry states in ABC trilayer graphene

Jeil Jung\* and Allan H. MacDonald

Department of Physics, University of Texas at Austin, USA

(Dated: August 2, 2012)

We use a self-consistent Hartree-Fock approximation with realistic Coulomb interactions for  $\pi$ -band electrons to explore the possibility of broken symmetry states in weakly disordered ABC stacked trilayer graphene. The competition between gapped and gapless broken symmetry states, and normal states is studied by comparing total energies. We find that gapped states are favored and that, unlike the bilayer case, gapless nematic broken symmetry states are not metastable. Among the gapped states the layer antiferromagnetic state is favored over anomalous and spin Hall states.

PACS numbers: 73.22.Pr, 71.15.Nc, 71.70.Gm, 73.22.Gk

## I. INTRODUCTION

The electronic structure of few layer graphene<sup>1,2</sup> systems consists of pairs of bands which cross, or narrowly avoid crossing, near the Fermi level. Because the number of band pairs depends in an interesting way on the stacking arrangement, and because both semi-metallic and semi-conducting behaviors occur, this family of two-dimensional materials provides an attractive playground for the study of electron interaction effects in systems<sup>3,4</sup> with approximate Fermi points. For example, interactions lead to a marginal Fermi liquid behavior in neutral single layer graphene,<sup>5,6</sup> and to broken-symmetry ordered states in bilayers.<sup>7-15</sup>

The recent surge of interest in ABC stacked trilayer graphene<sup>16-27</sup> motivates theoretical studies of the electron interaction induced instabilities that are expected when these structures are weakly disordered. Instabilities are favored in ABC trilayers by extremely flat crossing<sup>2</sup> of a single-pair of bands at the neutral system Fermi level, and by exchange energy frustration associated with momentum-space textures in the valence band wavefunctions.<sup>28</sup> In the trilayer case the competition between competing broken symmetry states is massaged by weak remote neighbor hopping processes that reshape the bands at energies within  $\sim 20$  meV of the crossing point.<sup>29</sup> This energy scale should be compared to the  $\sim 1$  meV scale of analogous processes in bilayer graphene<sup>30</sup>. The remote hopping processes are therefore more likely to play a prominent role in determining how the system responds to electron-electron interactions in the trilayer case.

The broken symmetry states that have been discussed in the bilayer graphene literature can broadly be classified either as gapped phases with broken layer inversion symmetry,<sup>7-10</sup> or as gapless nematic states that lower rotational symmetry.<sup>11</sup> Although the two types of states in principle should have clear experimental signatures, it has not yet been possible<sup>13-15</sup> to achieve a universally accepted consensus on the character of the ground state because of the complicating role of residual disorder. Studies of ABC stacked trilayer graphene could prove to be more unambiguous because its bands are flatter and interaction effects correspondingly stronger, while disorder strengths should be comparable.

In this paper we present a study of the competition between gapful and gapless states in ABC stacked trilayer graphene, including the effects of weak remote-hopping processes which

can dominate band dispersion very close to the band-crossing (Dirac) point. Our study is based on a six-band  $\pi$ -orbital tight-binding model, combined with long-range Coulomb interactions treated using a Hartree-Fock mean-field-theory. The quasiparticle band-structures of both gapped and gapless states are reshaped when interactions are included. We find that gapped phases are favored over a wide range of the hopping-parameter model space. In mean-field theory the energy difference between gapped and gapless states is typically smaller than  $\sim 10^{-7}$  eV per carbon atom. The small condensation energy reflects the fact that only single-electron states close to the band crossing points participate in ordering. The strength of the direct hopping process between low-energy sites on the outer layers of the trilayer,  $\gamma_2$ , plays an especially important role in determining the character of the ground state.

## II. MODEL HAMILTONIAN

We describe ABC trilayer graphene using a lattice model Hamiltonian with one atomic  $2p_z$  orbital per carbon site. We label the six sublattice sites illustrated in Fig. 1(a)  $A, B, A', B', A'', B''$ ; the  $A$  and  $B''$  sites avoid near-neighbor inter-layer coupling and for this reason are *low-energy sites* which are dominantly occupied by electrons close to the band crossing points. With this convention, the six band tight-binding model Hamiltonian of ABC trilayer graphene is:

$$H_0 = - \begin{pmatrix} 0 & \gamma_0 f & 0 & \gamma_3 f^* + \gamma_N & 0 & \gamma_2 \\ \gamma_0 f^* & 0 & \gamma_1 & 0 & 0 & 0 \\ 0 & \gamma_1 & 0 & \gamma_0 f & 0 & \gamma_3 f^* \\ \gamma_3 f + \gamma_N^* & 0 & \gamma_0 f^* & 0 & \gamma_1 & 0 \\ 0 & 0 & 0 & \gamma_1 & 0 & \gamma_0 f \\ \gamma_2 & 0 & \gamma_3 f & 0 & \gamma_0 f^* & 0 \end{pmatrix} \quad (1)$$

where

$$f(\mathbf{k}) = e^{ik_y a / \sqrt{3}} \left( 1 + 2e^{-i3k_y a / 2\sqrt{3}} \cos\left(\frac{k_x a}{2}\right) \right) \quad (2)$$

with  $a = 2.46\text{\AA}$  using the same triangular lattice vector convention as in Ref. [4,8]. The global minus sign in front of the Hamiltonian means that  $\pi$ -bonding bands have lower energy than anti-bonding bands when the  $\gamma$  parameters are positive.

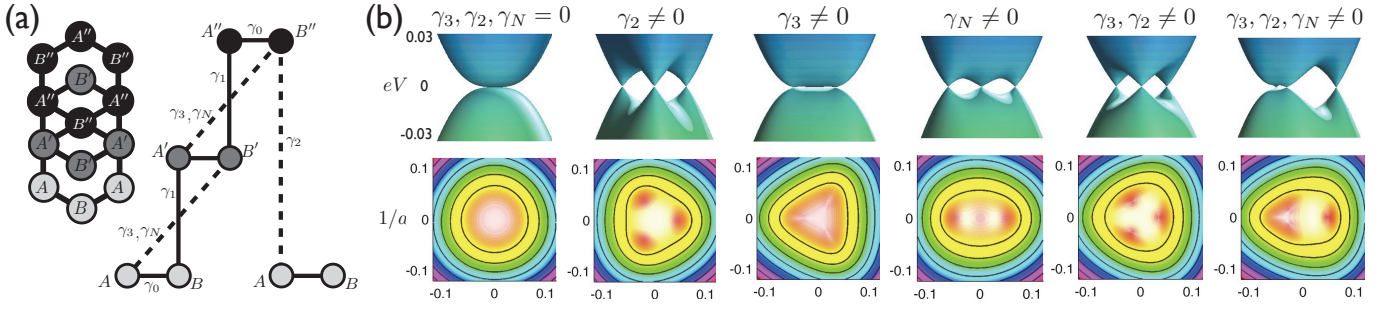


FIG. 1: Trilayer graphene unit cell and  $\pi$ -band structure. (a) Schematic representation of the hopping processes included in our model. (b) Band structure near the Dirac point  $K = (4\pi/3a, 0)$  for different values of the remote hopping parameters. The upper row shows 2D band structures seen from a view rotated by  $30^\circ$  with respect to vertical while the lower row shows the same information expressed in terms of contour plots. When non-zero, the hopping parameters have the values  $\gamma_2 = 0.01$  eV,  $\gamma_3 = 0.3$  eV. We have set  $\gamma_4 = \gamma_5 = 0$  throughout our calculations. Wave vectors  $k$  are in units of  $a^{-1}$ . The  $\gamma_2$  term splits the Brillouin-zone corner cubic band crossing into three Dirac cones (linear band crossings) located at the vertices of an equilateral triangle. The trigonal  $\gamma_3$  term acting on its own results in four band-crossing points, including one at the Brillouin-zone corner. When both terms are present simultaneously the gapless point at  $K$  disappears. When the signs of both terms are the same they tend to produce opposing triangular distortions, whereas if they have opposite signs their triangular distortions are reinforcing. The orientation of the triangular distortion for each of the above parameters is sign dependent. In realistic band structures the  $\gamma_2$  term dominates over  $\gamma_3$  resulting in three Fermi points with linear dispersion. The nematic term  $\gamma_N$  captures the influence of a layer relative-sliding strain and breaks the triangular rotational symmetry of the bands. We used the value  $\gamma_N^0 = 0.02$  eV in the above illustration.

In most of our calculations we have used graphite hopping parameter values which are similar to those in Ref. [31]:  $\gamma_0 = 3.12$  eV,  $\gamma_1 = 0.377$  eV,  $\gamma_2 = 0.01$  eV,  $\gamma_3 = 0.3$  eV. We specifically address the importance of the signs of the remote  $\gamma_2$  and  $\gamma_3$  hopping parameters. The near-neighbor intralayer and interlayer hopping processes  $\gamma_0$  and  $\gamma_1$  are responsible for broad features of the band structure, while the  $\gamma_2$  and  $\gamma_3$  parameters have their main impact close to the band-crossing points. This model qualitatively reproduces the *ab initio* band structure in Ref. [32], in particular capturing the orientation of the triangle formed by the three band-crossing points close to the Brillouin-zone corner. We have ignored the ABC trilayer  $\gamma_4$  and  $\gamma_5$  processes that break particle-hole symmetry, and other small onsite terms that are often introduced in models of graphite, because they do not visibly alter the low energy features of the bands in ABC trilayer graphene.

Using a model similar to that used previously for bilayer graphene,<sup>34,35</sup> we have also examined the influence of a term in the Hamiltonian that is intended to capture the influence on low-energy states of an interlayer relative-translation strain. We write  $\gamma_N = \gamma_N^0 \exp(-|\mathbf{k} - \mathbf{K}^{(l)}|/k_r)$ , introducing a damping factor which makes the term small away from the Brillouin-zone corners, where this form for the strain Hamiltonian becomes inaccurate, by setting  $k_r = \gamma_1/\hbar v_F = 0.0573 \text{ \AA}^{-1}$ .

Because there is some confusion in the literature on the signs of the remote hopping processes, we have also considered other sign choices for  $\gamma_2$  and  $\gamma_3$ . As shown in Fig. 1(b) direct hopping  $\gamma_2$  between the low energy sites  $A, B''$  gives rise to three Fermi points at the vertices of a triangle centered on the Brillouin-zone corner. The trigonal warping ( $\gamma_3$ ) process which connect the  $A, B'$  and  $A', B''$  sites is also responsible for a trigonal distortion that leads to four Fermi points

near  $K$ , as in bilayer graphene. Each one of the three Fermi points contribute to a phase winding of  $2\pi$  for a total  $6\pi$  phase winding along paths that encircle all three points, as expected in ABC trilayer graphene<sup>2</sup>. (We use the term Fermi point to refer to a band crossing that is tied to the Fermi level of a neutral ABC trilayer. The band crossing points are exactly at the Fermi level because we have neglected particle-hole symmetry breaking terms in the band structure model.) Both  $\gamma_2$  and  $\gamma_3$  terms break circular symmetry near the Dirac point by splitting a single Fermi point with cubic band dispersion into multiple Fermi points with linear dispersion. The orientations of the triangular distortion due to  $\gamma_2$  and  $\gamma_3$  are opposite when both hopping parameters have the same sign. First principles band structure calculations suggest that  $\gamma_2$  dominates over  $\gamma_3$  and determines the shape of the bands near the Dirac point. (Note that  $\gamma_2$  has a much greater influence on the two low-energy states than  $\gamma_3$  for a given numerical value because it couples them directly, whereas  $\gamma_3$  acts virtually via high-energy states.) When both terms are present simultaneously and have the same sign the band structure can have a hybrid shape; for some parameters values the bands consist of two intertwined triangles with opposite orientations that can exhibit up to nine Dirac cones. The additional parameter,  $\gamma_N$  couples  $A, B'$  and  $A', B''$ , like the  $\gamma_3$  term, but without an accompanying factor  $f(\mathbf{k})$ . The  $\gamma_N$  term qualitatively describes a band deformation that lowers the crystal rotational symmetry, and is similar to the model used to mimic a small layer-sliding structural deformation in bilayer graphene<sup>35</sup>. This term is also useful to seed lowered rotational symmetry gapless states in our Hartree-Fock calculations.

Electron-electron interaction effects are treated in an unrestricted Hartree-Fock approximation<sup>4,8</sup> which allows symme-

tries to be broken:

$$V_{HF} = \sum_{\mathbf{k}\lambda\lambda'} U_H^{\lambda\lambda'} \left[ \sum_{\mathbf{k}'} \langle c_{\mathbf{k}'\lambda'}^\dagger c_{\mathbf{k}'\lambda'} \rangle \right] c_{\mathbf{k}\lambda}^\dagger c_{\mathbf{k}\lambda} - \sum_{\mathbf{k}'\lambda\lambda'} U_X^{\lambda\lambda'} (\mathbf{k}' - \mathbf{k}) \langle c_{\mathbf{k}'\lambda'}^\dagger c_{\mathbf{k}'\lambda} \rangle c_{\mathbf{k}\lambda}^\dagger c_{\mathbf{k}\lambda'} \quad (3)$$

where  $c_{\mathbf{k}\lambda}^\dagger$ ,  $c_{\mathbf{k}\lambda}$  are Bloch state creation and annihilation operators, and  $\lambda = (l, \sigma)$  lumps lattice and spin indices. The Hartree and Exchange Coulomb integrals in Eq.( 3),

$$U_H^{ll'} = \frac{1}{A} \sum_{\mathbf{G}} e^{i\mathbf{G} \cdot (\mathbf{s}_l - \mathbf{s}_{l'})} \left| \tilde{f}(|\mathbf{G}|) \right|^2 \tilde{V}^{ll'}(|\mathbf{G}|) \quad (4)$$

$$U_X^{ll'}(\mathbf{q}) = \frac{1}{A} \sum_{\mathbf{G}} e^{i\mathbf{G} \cdot (\mathbf{s}_l - \mathbf{s}_{l'})} \left| \tilde{f}(|\mathbf{q} - \mathbf{G}|) \right|^2 \tilde{V}^{ll'}(|\mathbf{q} - \mathbf{G}|), \quad (5)$$

involve sums over reciprocal lattice vectors  $\mathbf{G}$ . In these equations  $\mathbf{s}_l$  is the (2D projection of the) position of the sublattice in the unit cell. We used an isotropic atomic orbital form factor  $\tilde{f}(\mathbf{q}) = \int d\mathbf{r} e^{-i\mathbf{q} \cdot \mathbf{r}} |\phi(\mathbf{r})|^2 = (1 - (r_o q)^2) / ((1 + (r_o q)^2)^4)$  with an artificially large atomic radius  $r_o = 3a_o / \sqrt{30}$  to account for  $sp_2$  orbital polarization.<sup>4</sup> Here  $a_o = a / (2\sqrt{3})$  is the covalent bond radius of carbon. The two-dimensional Coulomb interactions in Eqs. (4-5) are defined by  $\tilde{V}^{ll'}(\mathbf{q}) = 2\pi e^2 / (|\mathbf{q}| \epsilon_r)$  when the sublattice indices  $l$  and  $l'$  refer to the atoms in the same layer, and  $(2\pi e^2 / (|\mathbf{q}| \epsilon_r)) \exp[-|\mathbf{q}|d]$  when they refer to atoms in layers separated by a distance  $d$ .

We used an effective dielectric constant  $\epsilon_r = 4$  in our calculations, partly to account for dielectric screening by surrounding material and partly to account for the well known tendency of Hartree-Fock approximation, which neglects screening, to overestimate exchange interaction effects.<sup>33</sup> The present implementation of the lattice model Hartree-Fock mean-field theory follows closely the method described in Refs. [4,8] for single and bilayer graphene which also used a momentum space representation of the Coulomb interaction. One difference in the present implementation is that we sample the full Brillouin zone without taking advantage of the symmetry of the crystal in order to allow for the possibility of broken rotational symmetry nematic phases. Because of the greater importance of states near the Dirac point we have sampled momentum space non-uniformly; for  $\mathbf{k}$ -points closer than  $\sim 0.5/a$  to the Dirac point (where  $a = 2.46\text{\AA}$  is the triangular lattice constant of graphene) we have used a sampling density corresponding to  $2304 \times 2304$  points in the entire Brillouin zone. Outside this region we used a matched but coarser sampling with density corresponding to  $18 \times 18$  points in the Brillouin zone. For a given sampling density, the Hartree-Fock equations are solved iteratively and converged to  $\sim 10^{-11}$  eV per carbon atom in total energy.

### III. GAPPED AND GAPLESS STATES

As in the AB bilayer case, the low energy valence band states of ABC graphene are given approximately by equal weight coherent sums of top and bottom layer wavefunctions

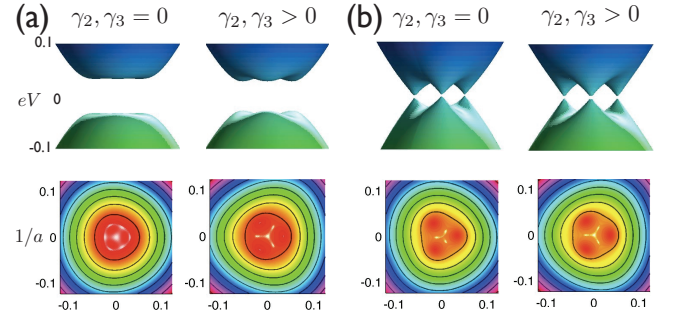


FIG. 2: Self-consistent Hartree-Fock calculations iterated from seeds for the gapped and gapless nematic states in ABC trilayer graphene. The gapped solution (a) has been obtained starting from the layer antiferromagnetic initial condition, while the gapless self-consistent solution (b) has been obtained by seeding with a nematic  $\gamma_N$  term. Note that the gapless solutions restore the rotational symmetry of the crystal lattice that was broken by the  $\gamma_N$  term, indicating that nematic order is not stable at the mean-field level in the trilayer case. When the remote hopping parameters  $\gamma_2 = 0.01$  eV and  $\gamma_3 = 0.3$  eV are accounted for they induce a triangular distortion of the bands near the Dirac point and determine the angles at which the band crossings occur. These processes do not have a large influence on the gapped ground state.

with momentum-dependent phase differences. The gapped broken symmetry states spontaneously increase weight in one of the two layers, whereas<sup>28</sup> the nematic states break the lattice rotational symmetry of the inter-layer phases. In the following we present the results of our  $\pi$ -band Coulomb-interaction Hartree-Fock study. This mean-field-theory calculation we perform cannot be fully quantitative because it accounts for screening in an ad-hoc way which might be quantitatively inaccurate, and because it neglects higher-order correlation effects. We believe though that our results provide some insight into the competition between different potential ordered states, and in particular into the way this competition is influenced by band structure features particular to ABC trilayer graphene. We first discuss the gapped states, which have spontaneous layer polarizations with spin or valley dependent signs, and then ungapped states with lowered rotational symmetry.

In a continuum model, the energy of the gapped states is minimized when half of the spin-valley components are polarized toward one layer and half to the other.<sup>8,9</sup> We consider only states of this type, which are favored over other closely related states by electrostatic interactions. In a lattice model there is a clear distinction and an energy difference between states with opposite layer polarizations for different valleys, which have either an anomalous Hall (AH) effect or a spin Hall (SH) effect, and states with opposite layer polarization for opposite spins (LAF), which form an antiferromagnetic state. The three types of ABC trilayer gapped states that have no overall layer polarization are compared in Table I. In our mean-field calculations anomalous Hall and spin Hall states have the same energy.

We define the condensation energy of the LAF and AH/SH

AF	( $\lambda_z$ $\tau_z$ $\sigma_z$ )	$\sigma_{xy}^{K,\uparrow}$	$\sigma_{xy}^{K',\uparrow}$	$\sigma_{xy}^{K,\downarrow}$	$\sigma_{xy}^{K',\downarrow}$
AH	( $T K \uparrow$ ) ( $B K' \uparrow$ ) ( $T K \downarrow$ ) ( $B K' \downarrow$ )	3	3	3	3
SH	( $T K \uparrow$ ) ( $B K' \uparrow$ ) ( $T K' \downarrow$ ) ( $B K \downarrow$ )	3	3	-3	-3
LAF	( $T K \uparrow$ ) ( $T K' \uparrow$ ) ( $B K \downarrow$ ) ( $B K' \downarrow$ )	3	-3	-3	3

	$\Delta n_l^{LAF}$	$\Delta n_l^{AH}$	$\Delta_{gap}^{LAF}$	$\Delta_{gap}^{AH}$	$\Delta E_{cond}^{LAF}$	$\Delta E_{cond}^{AH}$
$\gamma_2, \gamma_3 = 0$	1.22	1.21	65.1	64.9	-3.599	-3.554
$\gamma_2, \gamma_3 > 0$	1.09	1.08	56.0	55.6	-1.716	-1.680
$\gamma_2 < 0, \gamma_3 > 0$	0.12	0.10	12.1	11.7	0.00039	0.00046

	$\Delta E_{tot}$	$\Delta E_X$	$\Delta E_X^{KK}$	$\Delta E_X^{KK'}$
$\gamma_2, \gamma_3 = 0$	-4.43	-14.02	-2.62	-0.88
$\gamma_2, \gamma_3 > 0$	-3.58	-13.81	-2.77	-0.68
$\gamma_2 < 0, \gamma_3 > 0$	-0.0065	-1.660	-0.4154	0.0005

TABLE I: *Upper panel:* Mean-field theory properties of the three balanced-charge-density gapped states. Each of these states has two of the four valley/spin flavors polarized towards the top layer and two toward the bottom layer. Each polarized flavor contributes three quantized  $e^2/h$  units to the Hall conductivity with a sign that depends on both valley and layer polarization; the continuum model assignments can be retained in a lattice model because the momentum space Berry curvatures are strongly localized near Brillouin-zone corners. *Middle panel:* The density transfer from one outer layer to the other  $\Delta n_l$  for each valley-spin degree of freedom in units of  $10^{11} \text{cm}^{-2}$ . (This density scale corresponds to  $\sim 1.3 \cdot 10^{-5}$  electrons per carbon atom.) The total amount of charge transferred per valley-spin is larger in the more stable LAF configuration than the AH or SH configurations.  $\Delta_{gap}$  is the energy gap in meV. The condensation energies  $\Delta E_{cond} = E_{gapped} - E_{gapless}$  shown are differences between the ordered gapped and gapless normal phases in units of  $10^{-7}$  eV per carbon atom. The gapless normal state energies have been obtained from a self-consistent calculation starting from the band orbital seed. The anomalous Hall and spin Hall states have the same energy in mean-field theory. *Lower panel:* Differences in total energy between LAF and AH/SH states,  $\Delta E = E^{LAF} - E^{AH/SH}$ , in units of  $10^{-9}$  eV per carbon atom. The exchange energy difference per spin/valley is separated into an intravalley ( $\Delta E_X^{KK}$ ) and an intervalley ( $\Delta E_X^{KK'}$ ) contribution. Note that the total exchange energy difference satisfies  $\Delta E_X = 4(\Delta E_X^{KK} + \Delta E_X^{KK'})$ . Intervalley exchange, normally neglected in continuum models, makes a substantial contribution to the energy difference between LAF and anomalous Hall states.

gapped states as their energy relative to the ground state energy of the unbroken symmetry states. The unbroken symmetry state energy is determined by carrying out self-consistent mean-field calculations that are seeded by the non-interacting electron ground state. We find that the condensation energies for the ordered states are  $\sim 10^{-7}$  eV per carbon atom. The condensation energy is approximately three times smaller than the product of the energy gap  $\Delta_{gap}$  and the charge transferred between layers within individual spins and valleys  $\Delta n_l$ .

The condensation energy scales are approximately five times larger than those obtained for bilayer graphene<sup>8</sup> with similar approximations, presumably because the crossing bands are even flatter in the trilayer case, increasing the role of

interactions. The band gaps we calculate and present in Table I are roughly ten times larger than the the spontaneous gap values  $\sim 6$  meV estimated from transport measurements in ABC trilayer graphene<sup>16</sup>, and between 1.6 to 2 times larger than the gaps ( $\sim 30$  meV) obtained for the bilayer graphene using the same value of  $\epsilon_r = 4$ . [8] This could suggest that screening effects are underestimated by this value of  $\epsilon_r$ , or that other interaction effects than are absent in mean-field-theory play an essential role.

Experimentally the ratio of trilayer to bilayer gaps is  $\sim 2.5$ , close to the ratio we obtain. This suggests that the choice  $\epsilon_r = 4$  quantitatively overestimates exchange effects in both cases. The discrepancy between theory and experiment could, however, be due in part to the unfavorable influence of disorder in experimental samples, and also in part to inaccuracies in our band structure model. From the results in Table I we can observe, for example, that the gapped states are strongly suppressed when  $\gamma_2$  and  $\gamma_3$  have opposite signs, separating the Fermi points of the three Dirac cones. On the other hand, when  $\gamma_2$  and  $\gamma_3$  have the same sign,<sup>37</sup> the overall effect is that of restoring the approximate circular symmetry of the bands, enhancing the chances for a gapped phase.

Our calculations find that the nematic broken symmetry state is not stable in ABC trilayers. When we iterate the Hartree-Fock equations starting from a nematic seed, lattice rotational symmetry is restored at convergence. In both  $\gamma_2 = \gamma_3 = 0$ , and the more realistic  $\gamma_2, \gamma_3 \neq 0$  case, the same unbroken symmetry state with three band crossing points is reached for self-consistent calculations starting from either nematic or band seeds. This result is different from the one obtained in the graphene bilayer case, in which the same type of calculation yields a stable gapless state which lowers the crystal's rotational symmetry giving rise to a nematic order.<sup>36</sup>

The gapped solution of the Hartree-Fock equations lowers the total energy of the system by avoiding rapid in-plane  $xy$  rotation of the sublattice pseudospin direction near the band crossing point.<sup>7</sup> The gapless nematic phase lowers the total energy of the system by reducing the wavevector dependence of inter-site phase differences and introduces an anisotropic renormalization of the band velocity. The competition between the two broken symmetry phases depends on how much energy can be gained by reshaping the quasiparticle bands in two different ways. Fig. 2 shows the band structures obtained from self-consistent calculations with gapped and nematic seeds. The remote hopping terms introduce a triangular distortion in the shape of the bands near the Fermi energy, but do not greatly influence gapped state properties. These distortions will have important consequences for the electronic properties of doped ABC trilayers. It is noteworthy that the gapless phase within the minimal model develops a three Fermi point structure due to electron interactions alone, although it does not lower rotational symmetry. The inclusion of the  $\gamma_2, \gamma_3$  terms also plays a role in determining the orientation of the triangular deformation the bands undergo near the Dirac points in the gapless state.

Motivated by uncertainty in the values of the remote hopping process parameters, we have performed self-consistent calculations over a range of values of the  $\gamma_2, \gamma_3$  and  $\gamma_N$  pa-

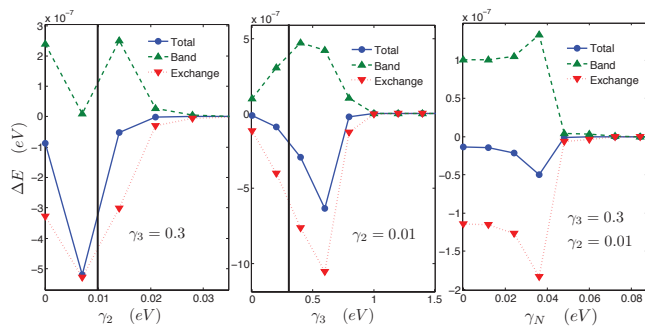


FIG. 3: (Color online) Energy difference between gapped and gapless states  $\Delta E = E_{\text{gapped}} - E_{\text{gapless}}$  as a function of  $\gamma_2$ ,  $\gamma_3$  and  $\gamma_N$ . For  $\gamma_N = 0$  the lattice symmetry of the gapless state is not lowered by interactions. The vertical black solid lines indicate the hopping parameters  $\gamma_2 = 0.01$  eV and  $\gamma_3 = 0.3$  eV that best approximate the band structure predicted by *ab initio* DFT calculations. For strong remote hopping processes, the gap in the gapped state closes progressively and the energy difference between gapped and ungapped states is reduced progressively.

rameters. The dependence of the energy difference between the interaction driven gapped and gapless states on model parameters is summarized in Fig. 3. We find that the gapped phase almost always has a lower total energy than the gapless phase. However, as expected, when the remote hopping processes are stronger, the difference in the total energy between the gapped and gapless phases become smaller. Fig. 3 shows that the occurrence of the gapped phase relies on the principal intra and interlayer processes whose strength is defined by  $\gamma_0$  and  $\gamma_1$ , and by the flatness of the crossing between conduction and valence bands that their dominance implies.

#### IV. DISCUSSION

We have used Hartree-Fock mean-field-theory calculation to demonstrate that electron interactions can lead to ordered phases in ABC trilayer graphene, provided that the strengths of remote hopping process in this two-dimensional crystal are close to current estimates. In ABC trilayers, bands near the Dirac point are strongly influenced by the  $\gamma_2$  parameter over energy scales of  $\sim 20$  meV, compared to the  $\sim 1$  meV scale over which analogous processes play a role in AB bilayers. The physics of their interplay with interactions is therefore less likely to be distorted by disorder. Remote hopping processes in ABC trilayers can be important in fixing the shape of the energy bands near the Fermi level. We have shown that the gapped broken symmetry phases are nevertheless preferred energetically over gapless states for a wide range of remote hopping parameters. We find that our gapless solutions

do not lower the crystal symmetry, although they do generally lead to the formation of a triple Dirac point at the vertices of an equilateral triangle. The nematic phase that would break the triangular crystal symmetry is not stable. When remote hopping processes are included the location of the Dirac points is fixed by the  $\gamma_2$  process.

There are three distinct gapped states which have very similar energies. Among these the anomalous Hall and spin Hall (AH and SH) states have the same energy within mean-field theory, whereas the layer antiferromagnet state is distinct and is favored by inter-valley exchange because electrons with the same spin state have the same sense of layer polarization. We find that the difference in total energy between LAF and AH/SH is two orders of magnitude smaller than the condensation energy of either state. These states should therefore, in our view, be considered as close cousins. It seems likely that real samples are likely to be found in configurations in which several phases are present separated by domain walls. An external magnetic field which favors anomalous Hall states, at least at finite carrier densities, likely can be used to manipulate the domain structure.

Using the Hartree-Fock approximation and reducing interaction strengths by a factor of  $\epsilon_r = 4$ , we find that ABC trilayer graphene has a substantial interaction driven gap of the order of 65 meV. The size of the gap is sensitive to the choice we have made for the  $\epsilon_r$  parameter, which we have chosen to mimic exchange interaction renormalization parameters that are used in *ab initio* hybrid-density-functional calculations. Band structure effects can reduce the size of the gap, substantially so when  $\gamma_2$  is assigned a negative value. For favorable parameters the gaps we find are approximately twice as large as than those predicted values for bilayer graphene using corresponding approximations. The theoretical gaps are therefore very much larger than initial estimates of a spontaneous band gap from ABC trilayer experiments which suggest a value  $\sim 6$  meV.<sup>16</sup> The discrepancy is certainly due in part to disorder and inhomogeneity which reduces the gaps of experimental systems below ideal values, but could also reflect a theoretical overestimate. We note in this connection that ABC trilayer graphene samples generally have poorer quality than bilayers. This difference could be due to lower effectiveness of the current annealing procedure routinely applied to suspended graphene single or multilayer samples. Future experimental work may establish a higher lower bound for the trilayer graphene gap.

#### Acknowledgments

This work was supported by SWAN, by Welch Foundation grant TBF1473, and by DOE Division of Materials Sciences and Engineering grant DE-FG03-02ER45958.

\* Electronic address: jeil@physics.utexas.edu

<sup>1</sup> F. Guinea, A. H. Castro Neto, and N. M. R. Peres, Phys. Rev. B

73, 245426 (2006); H. Min and A. H. MacDonald, Phys. Rev. B 77, 155416 (2008).



- <sup>2</sup> H. Min and A. H. MacDonald, Prog. Theor. Phys. Suppl. 176, 227 (2008).
- <sup>3</sup> A. A. Abrikosov and S. D. Beneslavskii, Zh. Eksp. Teor. Fiz. **59**, 1280 (1970) [Sov. Phys. JETP **32**, 699 (1971)].
- <sup>4</sup> J. Jung and A. H. MacDonald, Phys. Rev. B **84**, 085446 (2011).
- <sup>5</sup> J. Gonzalez, F. Guinea, and M. A. H. Vozmediano, Phys. Rev. B **59**, R2474 (1999); Phys. Rev. Lett. **77** 3589 (1996); Nucl. Phys. B **424**, 595 (1994).
- <sup>6</sup> D.D. Elias *et al.*, Nature Phys. **7**, 701 (2011) and work cited therein.
- <sup>7</sup> H. Min, G. Borghi, M. Polini and A. H. MacDonald, Phys. Rev. B **77**, 041407(R) (2008).
- <sup>8</sup> J. Jung, F. Zhang and A. H. MacDonald, Phys. Rev. B **83**, 115408 (2011).
- <sup>9</sup> F. Zhang, J. Jung, G. A. Fiete, Q. Niu and A. H. MacDonald, Phys. Rev. Lett. **106**, 156801 (2011).
- <sup>10</sup> F. Zhang, H. Min, M. Polini, and A. H. MacDonald, Phys. Rev. B **81**, 041402(R) (2010); arXiv:1205.5532 (2012); R. Nandkishore and L. Levitov, Phys. Rev. Lett. **104**, 156803 (2010); Phys. Rev. B **82**, 115124 (2010); Phys. Rev. B **82**, 115431 (2010); T. C. Lang *et al.*, arXiv:1207.3783v1; F. Freitag *et al.*, arXiv:1207.4424v1; F. Zhang *et al.*, arXiv:1205.5532v1; B. Wenzhong *et al.*, Proc. Nat. Ac. Sci. **109**, 10802 (2012); E. V. Gorbar, V. P. Gusynin, V. A. Miransky, I. A. Shovkovy, Phys. Rev. B **85**, 235460 (2012). M. Kharitonov, arXiv:1109.1553v2; G. Rutter *et al.*, Nature Physics **7**, 649 (2011);
- <sup>11</sup> O. Vafek and Kun Yang, Phys. Rev. B **81**, 041401(R) (2010); O. Vafek, Phys. Rev. B **82**, 205106, (2010); R. E. Thockmorton and O. Vafek, arXiv:1111.2076 (2011); V. Cvetkovic *et al.* arXiv:1206.0288 (2012).
- <sup>12</sup> M. M. Scherer, S. Uebelacker, and C. Honerkamp, Phys. Rev. B **85**, 235408 (2012); Y. Lemonik, I. L. Aleiner, C. Toke, V. I. Fal'ko, Phys. Rev. B **82**, 201408(R) (2010); Y. Lemonik, I. L. Aleiner, V. I. Fal'ko, Phys. Rev. B **85**, 245451 (2012).
- <sup>13</sup> J. Velasco *et al.*, Nature Nanotechnology **7**, 156, (2012); F. Freitag, J. Trbovic, M. Weiss and C. Schonenberger, Phys. Rev. Lett. **108**, 076602 (2012).
- <sup>14</sup> A. S. Mayorov *et al.* Science **333** (6044) pp. 860-863 (2011).
- <sup>15</sup> B. Feldman *et al.*, Nature Physics **5**, 889, (2009); R. Weitz *et al.* Science **330** (6005) 812 (2010).
- <sup>16</sup> W. Bao *et al.* Nature Physics **7**, 948 (2011).
- <sup>17</sup> L. Zhang *et al.* Nature Physics **7**, 953 (2011).
- <sup>18</sup> C. H. Lui *et al.* Nature Physics **7**, 944 (2011).
- <sup>19</sup> S. H. Jhang *et al.* Phys. Rev. B **84**, 161408(R) (2011).
- <sup>20</sup> M. Koshino, Phys. Rev. B **81**, 125304 (2010).
- <sup>21</sup> W. Norimatsu and M. Kusunoki, Phys. Rev. B **81** 161410, (2010).
- <sup>22</sup> L. Zhang *et al.*, Nature Physics **7**, 953 (2011).
- <sup>23</sup> J. H. Warner *et al.*, ACS Nano. **6**(6):5680 (2012).
- <sup>24</sup> C. H. Ho *et al.*, Ann. of Phys. **326**, 721 (2011).
- <sup>25</sup> S. Bala Kumar and J. Guo, Appl. Phys. Lett. **100**, 163102 (2012).
- <sup>26</sup> S. Yuan, R. Roldan, M. I. Katsnelson, Phys. Rev. B **84**, 125455 (2011).
- <sup>27</sup> F. Zhang, D. Tilahun, A. H. MacDonald, Phys. Rev. B **85**, 165139 (2012).
- <sup>28</sup> A. H. MacDonald, J. Jung and F. Zhang, Phys. Scr. T146, 014012 (2012).
- <sup>29</sup> M. Koshino and E. McCann, Phys. Rev. B **80**, 165409 (2009); F. Zhang, B. Sahu, H. Min, A. H. MacDonald, Phys. Rev. B **82**, 035409 (2010)
- <sup>30</sup> E. McCann and V. I. Fal'ko, Phys. Rev. Lett. **96**, 086805 (2006).
- <sup>31</sup> B. Partoens and F. M. Peeters, Phys. Rev. B **74**, 075404 (2006).
- <sup>32</sup> S. Latil and L. Henrard, Phys. Rev. Lett. **97**, 036803 (2006).
- <sup>33</sup> J. C. Slater, Phys. Rev. **81**, 385 (1951); A. Seidl, A. Görling, P. Vogl, J. A. Majewski, and M. Levy, Phys. Rev. B **53**, 3764 (1996).
- <sup>34</sup> Y.-W. Son, S.-M. Choi, Y. P. Hong, S. Woo, S. H. Jhi, Physical Review B **84**, 155410 (2011).
- <sup>35</sup> M. Mucha-Kruczynski, I. L. Aleiner, V. I. Fal'ko, Phys. Rev. B **84**, 041404 (2011).
- <sup>36</sup> J. Jung *et al.* In preparation.
- <sup>37</sup> J. Jung *et al.* In preparation.